THE JOURNAL OF BIOLOGICAL CHEMISTRY VOL. 281, NO. 10, pp. 6428–6433, March 10, 2006
© 2006 by The American Society for Biochemistry and Molecular Biology, Inc. Printed in the U.S.A.

Structural and Spectroscopic Studies Shed Light on the Mechanism of Oxalate Oxidase*

Received for publication, September 19, 2005, and in revised form, October 31, 2005 Published, JBC Papers in Press, November 15, 2005, DOI 10.1074/jbc.M510256200

Olaniyi Opaleye[‡1,2], Ruth-Sarah Rose[‡1], Mei M. Whittaker[§], Eui-Jeon Woo[‡3], James W. Whittaker[§4], and Richard W. Pickersgill[‡5]

From the [‡]School of Biological and Chemical Sciences, Queen Mary, University of London, Mile End Road, London E1 4NS, United Kingdom and the [§]Department of Environmental and Biomolecular Systems, OGI School of Science and Engineering, Oregon Health and Science University, Beaverton, Oregon 97006-8921

Oxalate oxidase (EC 1.2.3.4) catalyzes the conversion of oxalate and dioxygen to hydrogen peroxide and carbon dioxide. In this study, glycolate was used as a structural analogue of oxalate to investigate substrate binding in the crystalline enzyme. The observed monodentate binding of glycolate to the active site manganese ion of oxalate oxidase is consistent with a mechanism involving C–C bond cleavage driven by superoxide anion attack on a monodentate coordinated substrate. In this mechanism, the metal serves two functions: to organize the substrates (oxalate and dioxygen) and to transiently reduce dioxygen. The observed structure further implies important roles for specific active site residues (two asparagines and one glutamine) in correctly orientating the substrates and reaction intermediates for catalysis. Combined spectroscopic, biochemical, and structural analyses of mutants confirms the importance of the asparagine residues in organizing a functional active site complex.

Oxalate oxidase (OXO; EC 1.2.3.4)[6] catalyzes the oxidation of oxalate, reducing dioxygen to hydrogen peroxide and forming 2 mol of carbon dioxide (1–3): $(COOH)_2 + O_2 \rightarrow 2CO_2 + H_2O_2$.

Oxalate oxidase is widespread in nature and has been found in bacteria (4), fungi (1, 5), and various plant tissues (6). It has been detected in barley seedling roots during germination and in the leaves of mature barley plants in response to powdery mildew infection (6, 7), suggesting a role in plant signaling and defense. The enzyme has been purified to homogeneity from barley seedling roots and its N-terminal sequence determined, allowing the corresponding cDNA to be isolated and the complete primary sequence to be determined (3, 8). These developments led to the recognition that the enzyme, OXO, is identical to an important marker of grain development during germination of wheat called germin (3, 8). OXO is a member of a functionally diverse protein superfamily known as the cupins (9) or double stranded β-helix proteins (10). Barley OXO forms a hexamer that has extreme stability to heat and proteolysis (11).

Spectroscopic studies demonstrated that OXO requires manganese for catalysis (12) and subsequent crystallographic studies on the barley enzyme revealed the structure of the hexamer (Fig. 1*a*) and confirmed the presence of a mononuclear manganese center buried deep within its jellyroll β-barrel domain (13). The manganese is bound by the side chains of three histidines and one glutamate residue, as well as two water molecules that occupy adjacent positions in the roughly octahedral metal complex (Fig. 1*b*). Based on the lack of obvious optical absorption and the presence of a characteristic EPR spectrum, the manganese ion has been assigned as the reduced Mn(II) oxidation state in the resting enzyme (12). Spectroscopic studies using recombinant OXO expressed in *Pichia pastoris* confirmed the presence of Mn(II) in the resting recombinant enzyme and provided the first spectroscopic evidence for oxalate binding to the manganese (14). The EPR signal of the anaerobic substrate complex, like that of the native enzyme, lies near $g = 2$ and therefore represents a six-coordinate metal center, consistent with either monodentate coordination of oxalate, retaining one of the two water molecules, or bidentate coordination with expulsion of both waters. Mn(III) was present in the protein samples as a minor species and the addition of oxalate resulted in the production of carboxylate free radicals. However, no other free radicals were detected in the EPR experiments even under turnover conditions indicating that oxy radicals, if formed by the enzyme, do not escape the active site during turnover, implying a tight coupling of oxygen and oxalate chemistry in the catalytic cycle (14).

The need to establish the details of the catalytic mechanism of OXO and the importance of doing so for understanding the evolution of biological catalysis was highlighted in a recent review (15). In the present work we describe the crystal structure of a substrate-analogue binary complex that allows, for the first time, identification of residues that bind substrates and catalytic intermediates, observations that provide new insight in the mechanism of OXO.

EXPERIMENTAL PROCEDURES

Production of Native, Recombinant, and Mutant Oxalate Oxidase—Native barley OXO and recombinant barley OXO were produced and purified as described previously (11, 14).

Construction of Mutants—The plasmid pPICZBαOXO (14) was used as a template for the production of all mutational variants of OXO using QuikChange multi-site-directed mutagenesis procedure (Stratagene, La Jolla, CA). Two 5′-phosphorylated primers were used (5′-CTGGGTGTTTCCATGGCCCGTGTTGACTTC-3′ for N75A OXO and 5′-CTCCAGGAGGTACCGCCCCACCACACATCC-3′ for N85A OXO). Silent mutagenesis was used to introduce a synonymous codon

* This work was supported in part by funds from the Biotechnology and Biological Sciences Research Council and Higher Education Funding Council for England (to R. W. P.) and by National Institutes of Health Grant GM 42680 (to J. W. W.). The costs of publication of this article were defrayed in part by the payment of page charges. This article must therefore be hereby marked "*advertisement*" in accordance with 18 U.S.C. Section 1734 solely to indicate this fact.

The atomic coordinates and structure factors (codes 2ET1, 2ET7, and 2ETE) have been deposited in the Protein Data Bank, Research Collaboratory for Structural Bioinformatics, Rutgers University, New Brunswick, NJ (http://www.rcsb.org/).

[1] Both authors contributed equally to this work.

[2] Recipient of a Biotechnology and Biological Sciences Research Council CASE studentship funded in part by Dow AgroSciences.

[3] Current address: Systemic Proteomics Research Center, Korea Research Inst. of Bioscience and Biotechnology, Taejon 305-333, Republic of Korea.

[4] To whom correspondence may be addressed: Dept. of Environmental and Biomolecular Systems, OHSU, 20000 N.W. Walker Rd., Beaverton, OR 97006-8291. Tel.: 503-748-1065; Fax: 503-748-1464; E-mail: jim@ebs.ogi.edu.

[5] To whom correspondence may be addressed. Tel.: 44-20-7882-6360; Fax: 44-20-8983-0973; E-mail: richard.pickersgill@qmul.ac.uk.

[6] The abbreviation used is: OXO, oxalate oxidase.

Downloaded from www.jbc.org at KING'S COLLEGE LONDON on October 22, 2007

TABLE 1
Crystallographic statistics

Crystal details	Native OXO	Recombinant OXO	$Asn^{75} \rightarrow Ala$ OXO
Space group	R32	F432	R32
Soak	10 mM glycolate	10 mM glycolate	None
Data collection			
Resolution range (Å)[a]	40–1.60 (1.66–1.60)	140–1.75 (1.81–1.75)	65–1.70 (1.79–1.70)
Unique reflections	23,143	64,382	19,027
Completeness (%)[a]	97.6 (98.4)	100.0 (100.0)	98.7 (99.7)
Multiplicity	15.0 (9.0)	14.4 (12.9)	10.0 (8.8)
R_{merge} $(I)^{a,b}$	2.5 (4.7)	7.3 (28.4)	7.2 (14.4)
Mean $I/\sigma(I)^a$	39.9 (26.1)	33.3 (9.8)	25.9 (14.7)
Refinement			
R-Factor[c] (%)	17.4	17.6	16.5
R-Free[c] (%)	20.0	18.8	21.1
DPI[d] (Å)	0.0897	0.0800	0.1099
Most favored φ/ψ(%)[e]	88.2/11.8	88.8/11.2	89.4/10.6
r.m.s.d. bond distances (Å)[f]	0.012 (0.022)	0.014 (0.022)	0.012 (0.022)
r.m.s.d. bond angles (°)[f]	1.372 (1.980)	1.392 (1.990)	1.422 (1.979)
Model			
Protein residues	201	402[g]	201
Manganese ions	1	2[g]	1
Waters	164	308[g]	221
GlcNAc	0	2[g]	0
Mean protein B-factor (Å^2)	8.2	15.3	13.1
r.m.s.d. compared with 1FI2(Å)[h]	0.173	0.221	0.293

[a] Values in parentheses are for the final shell.
[b] $R_{merge} = \Sigma_{hkl}\Sigma_i|I_i - \langle I\rangle|)/\Sigma_{hkl}\Sigma I_i$, where I_i is the intensity of the ith observation, $\langle I\rangle$ is the mean intensity of the reflection, and the summations extend over all unique reflections (hkl) and all equivalents (i), respectively.
[c] The R-factor $= \Sigma_{hkl}|F_o - F_c|/\Sigma_{hkl}|F_o|$, where F_o and F_c represent the observed and calculated structure factors, respectively. R-Factor is calculated using 95% of the data included in refinement and R-free the 5% excluded.
[d] Diffraction-component precision index.
[e] From PROCHECK, most favored/additionally allowed (24).
[f] Target σ in parentheses.
[g] Two subunits in the asymmetric unit.
[h] Root mean square deviation (r.m.s.d.) compared with native structure (13).

substitution (GGA for GGT) in the latter avoid predicted strong secondary structure in the primer. Sequences of the mutant plasmids were verified by DNA sequence analysis (Molecular Biology Core Facility, Oregon Regional Primate Research Center, Beaverton, OR). The mutant proteins were expressed in *P. pastoris* and purified using methods previously developed for recombinant OXO (14).

Crystallization, Crystal Soaks, and Data Collection—Crystals were grown using the hanging-drop vapor diffusion method at 18 °C using 1 μl of protein (10–15 mg/ml) plus 1-μl reservoir drops and 1-ml reservoirs. Native crystals grown from 2.3 M $(NH_4)_2SO_4$ and 5% 2-propanol were rhombohedral, R32 with a = 96.3 Å, c = 108.1 Å (hexagonal setting) and with one subunit in the asymmetric unit. Crystallization conditions for recombinant and mutant enzymes were derived independently from the conditions previously reported for native OXO (11, 13). Crystals of recombinant protein, grown from 10% polyethylene glycol 4000 and 0.1 M NaAc, pH 4.6, were tetragonal F432 with a = 250.4 Å and with two subunits in the asymmetric unit. Crystals of $Asn^{75} \rightarrow Ala$ OXO were grown from 20% 2-propanol, 0.1 M NaAc, pH 4.6, 0.2 M $CaCl_2$ and could be cryo-cooled directly. The $Asn^{75} \rightarrow$ Ala OXO crystals were similar to native crystals rhombohedral R32 with a = 94.8 Å, c = 106.2 Å (hexagonal setting) and with one subunit in the asymmetric unit. Native and recombinant crystals were soaked in reservoir solution supplemented with 10 mM glycolate for 20 min before rapid transfer through a solution supplemented with both 10 mM glycolate and 25% glycerol prior to cryo-cooling and data collection.

Crystallographic Calculations—Data from the native soaked crystal were collected using station PX9.6 at Synchrotron Radiation Source Daresbury and reduced and scaled using DENZO and SCALEPACK (16). Data from recombinant and $Asn^{75} \rightarrow$ Ala mutant crystals were collected using station PX 14.1 at Synchrotron Radiation Source Daresbury and reduced using MOSFLM (17) and SCALA (18). The quality of

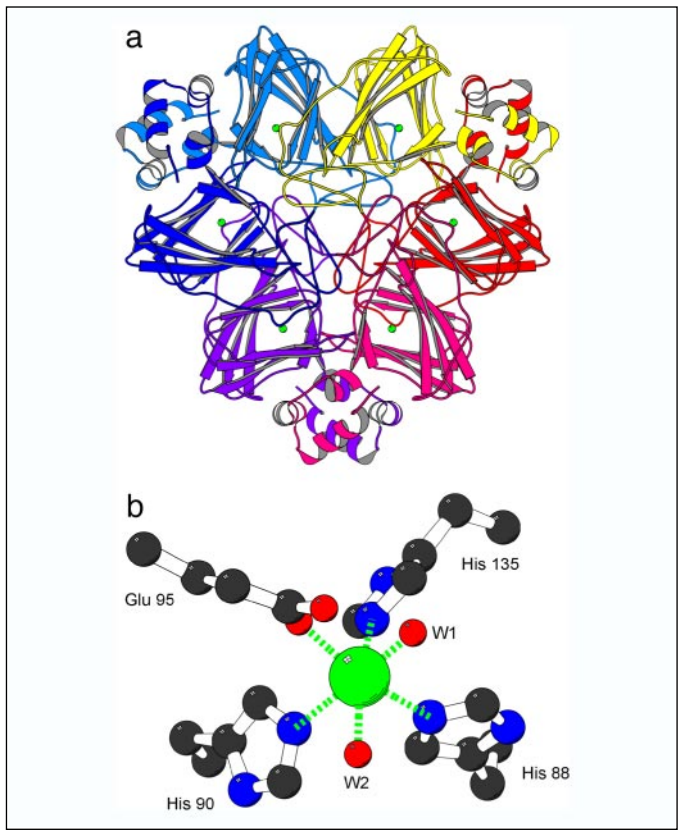

FIGURE 1. *a*, oxalate oxidase comprises a trimer of dimers with one active site manganese ion per protein subunit. *b*, octahedral coordination of the manganese ion at the catalytic center of the oxalate oxidase subunit is by three histidines, one glutamate, and two water molecules. This figure was prepared using MOLSCRIPT (29).

Downloaded from www.jbc.org at KING'S COLLEGE LONDON on October 22, 2007

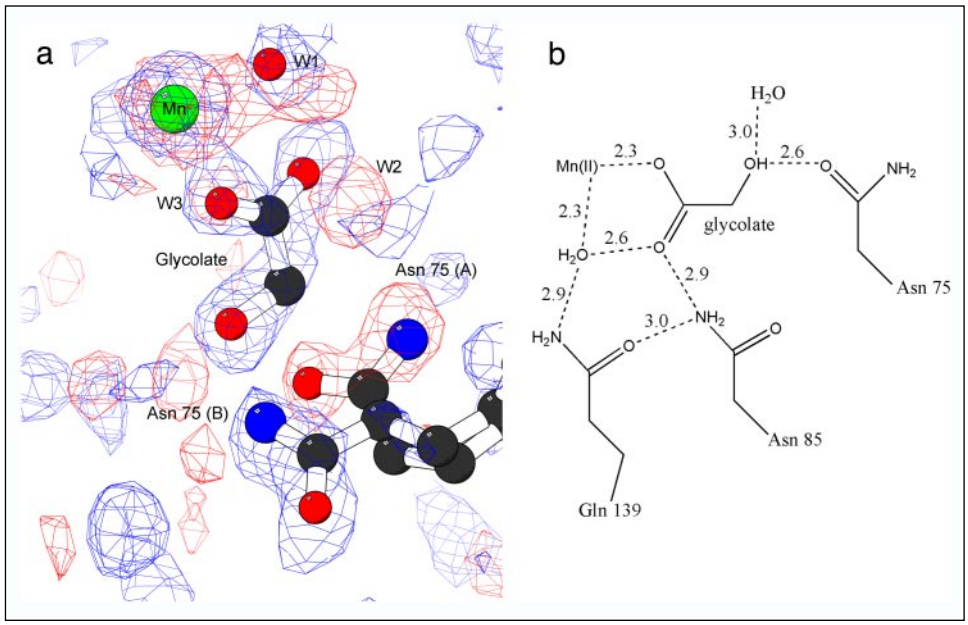

FIGURE 2. *a*, difference map revealing monodentate binding of glycolate to the active site manganese and movement of Asn^{75}. Positive electron density (+1 σ) is shown in *blue* and *negative* density (−1 σ) in *red*. Asn^{75} (*A*) labels the conformation present in native crystals, and Asn^{75} (*B*) labels the conformation seen in the glycolate complex. Additional changes in density are due to the movement of water molecules. There is clear evidence for the binding of glycolate and the expulsion of two waters from the active site (labeled W2 and W3), W1 remains bound to the manganese ion. This figure and Fig. 4 were prepared using BOBSCRIPT (30). *b*, schematic drawing of the network of interactions between oxalate oxidase and glycolate, distances are given in Å units.

TABLE 2
Specific activity for wild type and asparagine mutants

Sample	Specific activity[a]			
	No addition	1 M NH_4Cl	1 M NaCl	1 M Formamide
	μmol/min/mg protein			
WT OXO[b]	10.26 ± 0.85	7.29 ± 0.15	8.42 ± 0.10	10.61 ± 0.48
N75A OXO	0.24 ± 0.04	0.34 ± 0.02	0.38 ± 0.01	0.235 ± 0.014
N85A OXO	0.055 ± 0.004	0.132 ± 0.005	0.181 ± 0.004	0.048 ± 0.002

[a] Initial velocity measured using a thermostated (25 °C). Clark oxygen electrode calibrated with the protocatechuic acid/protocatechuate dioxygenase reaction (25).
[b] Recombinant barley oxalate oxidase expressed by *P. pastoris*.

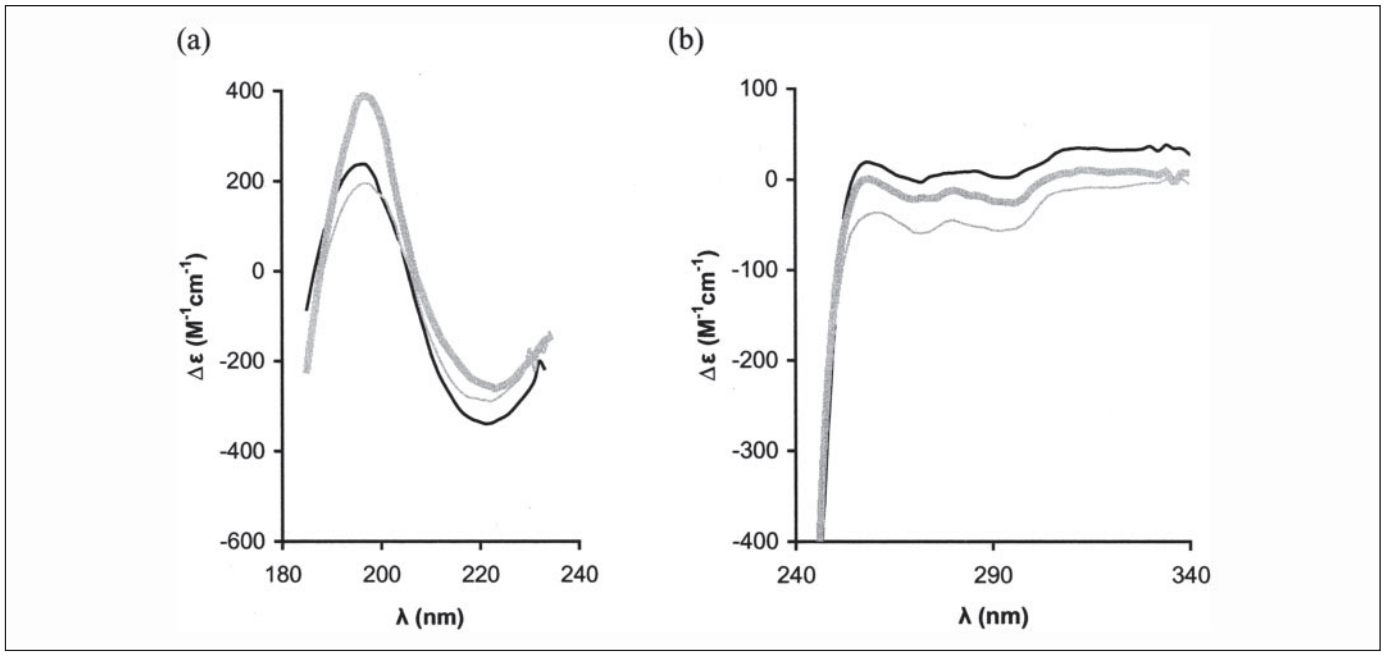

FIGURE 3. **Far-uv and near-uv circular dichroism spectra (*a*) and (*b*), respectively, of native and mutant oxalate oxidases (native shown as a *full black line*, N75A as a *thin gray line*, and N85A as a *thick gray line*).** The similarity of the CD spectra supports the view that the structures are closely similar and that the loss of activity seen for the mutants (Asn^{75} → Ala and Asn^{85} → Ala) is due to the loss of hydrogen bonding potential of the aparagine side chains.

the data and the extent of diffraction are presented in Table 1. Crystallographic calculations used the CCP4 programs (18) and the graphics program O (19). Difference Fourier maps were calculated using protein phases calculated from the native oxalate oxidase structure (Protein Data Bank accession code: 1FI2). The structure of glycolate was obtained from the CDS (20, 21). MOLREP (22) was used for molecular

Downloaded from www.jbc.org at KING'S COLLEGE LONDON on October 22, 2007

replacement calculations to determine the structure of recombinant OXO and REFMAC (23) was for the refinement of the three structures. 5% of the data were excluded from the refinement for the calculation of *R*-free. For the R32 crystals, the same reflections were used for calculating *R*-free as were used for the original structure determination but expanded where the data have higher completeness. The manganese-ligand distances were not restrained during refinement and the final models were validated using PROCHECK (24). A summary of the final structures and their geometry is given in Table 1.

Activity Measurements—OXO activity was measured using a thermostated Clark oxygen electrode calibrated with the protocatechuic acid/protocatechuate dioxygenase reaction (25). Initial velocity measurements of oxygen uptake were obtained with 20 mM oxalic acid in 50 mM sodium succinate buffer, pH 4 at 25 °C. The activity was also measured in the presence of 1 M NH_4Cl, 1 M NaCl and 1 M formamide in the assay mixture. Results of activity measurements are shown in Table 2.

Spectroscopy—Electron paramagnetic resonance spectra were recorded on a Bruker E500 X-Band EPR spectrometer with a SuperX microwave bridge and SHQ resonator equipped with a nitrogen flow cryostat. CD spectra were recorded using an Aviv Circular Dichroism Spectrophotometer Model 202 and processed using Dichroweb (26).

RESULTS AND DISCUSSION

Glycolate Binding in the Crystal—The manganese ion at the active center of OXO is bound by three histidines, one glutamate, and two waters (Fig. 1*b*). Each of the three histidines coordinates via the N-ϵ atom requiring the histidines to adopt the less-favorable Nδ-H tautomeric form. The sp^2 lone pair of each of the nitrogen atoms coordinates the manganese in an in-plane and head-on approach. The stereochemistry of the carboxylate-manganese ion coordination is *syn* corresponding to the more basic of the carboxylate oxygen sp^2 lone pairs. Although in principle the full range of oxidation states from 3− to 7+ is accessible to manganese, normally 2+ to 5+ is considered relevant to biological systems with the 2+ oxidation state the most stable and it is this high-spin Mn(II) ($S = 5/2$) oxidation state that is revealed by EPR spectroscopy of OXO (12, 14). Our crystallographic results show that glycolate binds to the manganese ion using one carboxylate oxygen in-plane with *syn* stereochemistry displacing one of the coordinating water molecules from the active site (Fig. 2). The second carboxylate oxygen forms a hydrogen bond with the remaining manganese-bound water molecule, the in-plane geometry indicating involvement of the more basic *syn* lone pair on the carboxy-oxygen. The non-coordinated carboxylate oxygen is also within hydrogen bonding distance of Asn^{85}, although Asn^{85} is more nearly perpendicular to the plane of the carboxylate. At the other end of the glycolate molecule, distal from the manganese, the hydroxyl hydrogen bonds Asn^{75}. Asn^{75} changes conformer to make this hydrogen bond, but it is not clear if Asn^{75} is accepting or donating a hydrogen bond as the other groups involved in completing the hydrogen bonding for both the glycolate hydroxyl and Asn^{75} are water molecules. The conformational flexibility of the Asn^{75} side chain reflected in these structures suggests a possible dynamic role for Asn^{75} mobility in catalysis, perhaps assisting movement of substrates and products through the access channel. In addition to Asn^{75} and Asn^{85}, the network of hydrogen bonds anchoring glycolate in the OXO active site also includes another side chain, Gln^{139}, which hydrogen bonds to both Asn^{85} and the manganese-bound water molecule (Fig. 2).

The mode of glycolate binding observed in the protein crystal is distinct from that observed in small molecule inorganic complexes of Mn(II) and glycolate (27). In the latter case, the hydroxy acid exhibits bidentate coordination *via* both carboxylate and hydroxyl functions, requiring *anti*-stereochemistry for the carboxylate-metal interactions. The fact that the protein complex exhibits the extended, monodentate coordination mode suggests a specific stabilization of this structure in the active site, including steric barriers disfavoring bidentate coordination. Modeling the binding of oxalate in bidentate coordination within the OXO structure results in steric clashes with the side chains of Leu^{77} and Met^{149}.

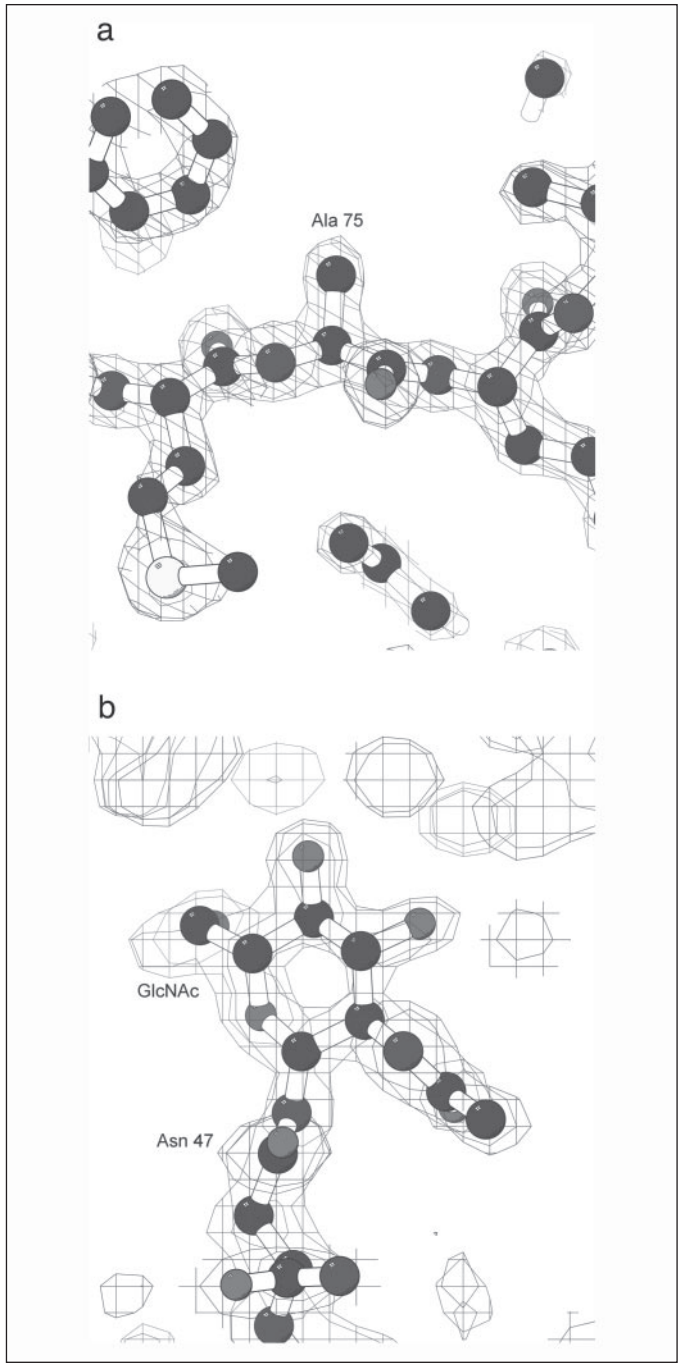

FIGURE 4. *a*, the electron density for Ala^{75} in $Asn^{75} \rightarrow$ Ala OXO. Negligible changes in structure accompany this mutation so the loss of activity is directly due to the loss of the asparagine side chain rather than any indirect cause. *b*, the presence of GlcNAc attached to asparagine 47 accounts for the crystallization of the recombinant protein in space group F432 as opposed to R32 native and mutant OXO (see also Table 1). There is clear evidence for a single GlcNAc in both the A and B subunits of the recombinant protein, and the final model is shown together with the original SIGMAA weighted 2–1 map contoured at 1 σ.

Downloaded from www.jbc.org at KING'S COLLEGE LONDON on October 22, 2007

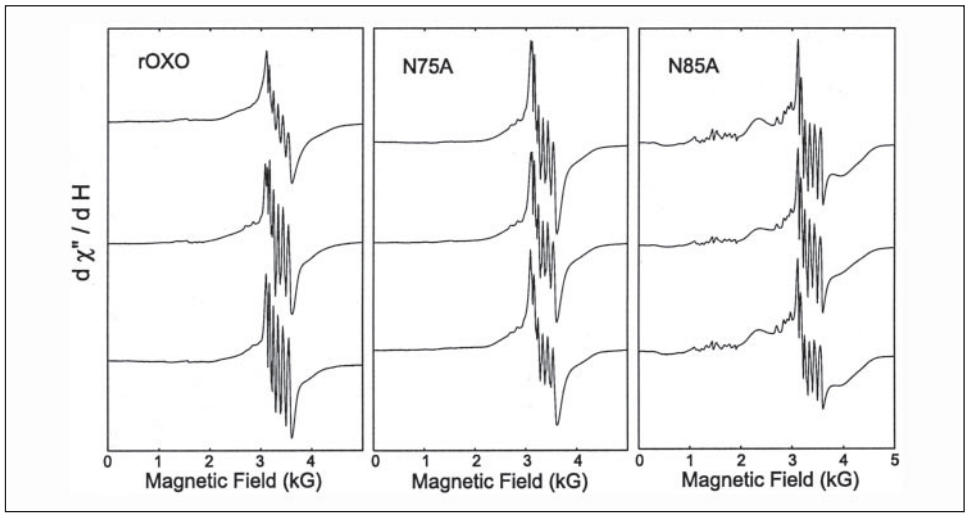

FIGURE 5. **EPR spectra for anaerobic rOXO complexes.** *a–c*, wild type rOXO (1.5 mM protein, 0.32 mM manganese) (*a*) N75A rOXO (2.8 mM protein, 0.35 mM manganese) (*b*), and N85A rOXO (2 mM protein, 0.55 mM manganese) (*c*, *right*) in 50 mM potassium succinate buffer, pH 4. *Top*, ligand-free protein solution; *middle*, in the presence of 20 mM sodium oxalate; *bottom*, in the presence of 10 mM sodium glycolate. Experimental conditions: frequency, 9.39 GHz; modulation amplitude, 10 G; power, 5 milliwatt; temperature, 130 K.

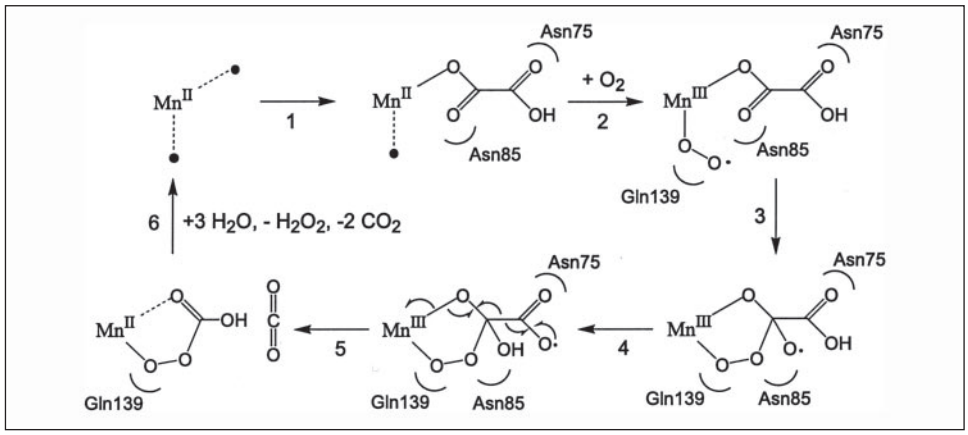

FIGURE 6. **Proposed catalytic mechanism for oxalate oxidase.** *Step 1*, monodentate coordination of oxalate monoanion displaces one solvent molecule from the Mn(II) center. *Step 2*, dioxygen binds directly to Mn(II) in a site to form a Mn(III) superoxide metalloradical complex, stabilized by Gln^{139}. *Step 3*, superoxide nucleophile adds to the proximal carboxyl group, activating the substrate. *Step 4*, hydrogen atom transfer forms a distal carboxyl radical species. *Step 5*, the substrate free radical rearranges with homolytic C–C bond cleavage and reduction of Mn(III) to Mn(II). *Step 6*, release of products may include hydrolysis of percarbonate.

The oxalate complex of OXO is expected to closely resemble the glycolate complex, although a small rotation of the molecule would be required to accommodate the additional oxygen atom of oxalate. This rotation, a small anti-clockwise rotation in the plane of Fig. 2*b* maintaining the manganese coordination, would enlarge the binding site occupied by water W1 creating a potential dioxygen-binding site (see below). The asparagines and glutamine appear to be essential for maintaining the two substrates in the correct orientation for catalysis. This is confirmed by the almost complete loss of activity for both the $Asn^{75} \rightarrow Ala$ and $Asn^{85} \rightarrow Ala$ mutations (Table 2), and the lack of glycolate binding in the crystals of the mutant proteins, as well as in solution (see below). The CD spectra of $Asn^{75} \rightarrow Ala$ OXO is identical to the native spectra (Fig. 3) and more convincingly the crystal structure is nearly identical except for the alanine for asparagine substitution (Fig. 4*a*; Table 1). These results establish the direct involvement of Asn^{75} in binding and catalysis. In broad terms Asn^{75}, Asn^{85}, and Gln^{139} are poised to hold the carboxylic substrate and dioxygen in the correct orientation with respect to the manganese for catalysis. Asn^{75} and Asn^{85} can also stabilize catalytic intermediates, while Asn^{85} and Gln^{139} ensure the manganese, carboxylate, and dioxygen radical are planar to direct the formation of the percarbonate product.

Glycolate and Oxalate Binding in Solution—The Mn(II) EPR spectra for anaerobic recombinant OXO complexes in the presence of glycolate and oxalate show perturbations to the metal ion suggesting a change in manganese coordination (Fig. 5) that is not seen with either of the asparagine mutants. The average hyperfine splitting of the Mn(II) sextet is 86 G for rOXO, 92 G in the presence of oxalate, and 90 G in the presence of glycolate. In contrast, the Mn(II) EPR spectra for OXO $Asn^{75} \rightarrow Ala$ and $Asn^{85} \rightarrow Ala$ are unchanged by addition of either oxalate or glycolate, implying that the substrate and analogue do not bind to these mutational variants under the conditions of the EPR experiment (Fig. 5). This is consistent with involvement of the asparagines in stabilizing the complex and possibly controlling the geometry of the interaction between manganese and oxalate so as to confer productive binding.

Activity Measurements and Rescue Experiments—Steady-state oxygen uptake measurements demonstrate that substitution of alanine for either Asn^{75} or Asn^{85} dramatically reduces OXO activity to 2.4 and 0.5%, respectively, of the wild type level (Table 2). The activity was not restored in the presence of hydrogen-bonding solutes (ammonium ion, formamide). Higher activity observed in the presence of ammonium chloride can be accounted for as a result of nonspecific ionic strength effects, or specific chloride effects, since a similar enhancement was observed with sodium chloride for both $Asn^{75} \rightarrow Ala$ and $Asn^{85} \rightarrow Ala$ mutants. These results indicate that the loss of function associated with the $Asn^{75} \rightarrow Ala$ and $Asn^{85} \rightarrow Ala$ substitutions cannot be easily rescued by exogenous hydrogen bonding agents. For wild type OXO, glycolate did not serve as a substrate and did not significantly inhibit turnover when included in the assay at equimolar (20 mM) concentrations of oxalate, implying that glycolate is bound less tightly than the substrate, oxalate.

Structure of Recombinant OXO and Mutants—OXO crystals grown using fresh protein appear well formed but do not diffract. Over time the extent of glycosylation of OXO spontaneously decreases, as judged by the considerably less smeared appearance of the OXO band on an SDS-

Downloaded from www.jbc.org at KING'S COLLEGE LONDON on October 22, 2007

PAGE, and under appropriate conditions the form of OXO containing a single GlcNAc on Asn^{47} (Fig. 4*b*) crystallizes in F432 with two molecules in the asymmetric unit or the fully deglycosylated OXO crystallizes in R32 with a single molecule in the asymmetric unit. The structure of glycolate complex in recombinant OXO crystals is identical to that described above for the native enzyme (Table 1; Fig. 2).

Implications for Oxalate Oxidase Mechanism—These combined structural and biochemical studies provide the basis for a novel mechanism of oxalate oxidase catalysis, incorporating the new insights into carboxylate coordination modes and functions of specific catalytic residues (Fig. 6). Oxalate oxidase binds the singly ionized oxalate monoanion as substrate at the optimum pH for the enzymatic reaction (pH = 4), which lies between the two pK_a values for oxalic acid dissociation ($pK_{a,1}$ = 1.25, $pK_{a,2}$ = 4.14) (Fig. 6). The singly charged oxalate may be expected to bind to OXO in the same fashion as glycolate, although a slight rotation of oxalate would be required to accommodate the additional oxygen atom of the non-coordinated carboxyl group of oxalate. In this geometry, a possible dioxygen binding site is created in the active site, comprising the reduced Mn(II) metal ion and the Gln^{139} side chain. Monodentate coordination of oxalate allows dioxygen to bind in the inner sphere of the Mn(II) ion in place of water (W1 in Fig. 2), stabilizing reduced oxygen species that are predicted to occur as reaction intermediates during turnover through direct coordination to the metal ion. The binding of oxalate carboxylate not only forms the dioxygen binding site but also, by altering the electrostatic potential of the metal environment, will lower the redox potential of the Mn(II)-Mn(III) couple. The metal ion is thus activated to bind dioxygen as a superoxide anion coupled to oxidation of Mn(II) to Mn(III) (Fig. 6, *step 2*). A hydrogen-bonding network anchored on the amide side chains of Asn^{75}, Asn^{85}, and Gln^{139} appears to be essential for correctly orienting dioxygen and oxalate substrates relative to the manganese ion. The nucleophilic superoxide metalloradical generated in this reaction would be positioned to add to the adjacent oxalate carboxylate (Fig. 6, *step 3*), generating a transient substrate oxyradical and activating oxalate for C–C bond cleavage. One possible pathway is illustrated in Fig. 6, showing migration of the free radical to the distal, non-coordinated carboxyl group by hydrogen atom transfer (Fig. 6, *step 4*), followed by radical-induced decarboxylation involving homolytic C–C bond cleavage and reduction of Mn(III) to Mn(II) (Fig. 6, *step 5*). This leads to formation of peroxycarbonate as an initial product of the reaction. Release of CO_2 and percarbonate, or a second molecule of CO_2 and hydrogen peroxide formed by subsequent hydrolysis of percarbonate, completes the turnover cycle. In this scheme, Asn^{75} and Asn^{85} contribute the hydrogen-bonding framework stabilizing the reaction intermediates, and Asn^{85} and Gln^{139} are appropriately positioned to facilitate formation of percarbonate product by ensuring the necessary planarity of the manganese ion and atoms of the dioxygen superoxide and the CO_2 fragment from oxalate (Fig. 6). As drawn, with the carboxy-oxygen hydrogen bonding to Asn^{75}, Asn^{85} is positioned to encourage both the conversion of geometry of the C1 of oxalate from sp^2 to sp^3 (Fig. 6, *step 3*) and the hydrogen atom transfer (Fig. 6, *step 4*).

The recent crystal structure of the hypothetical oxalate decarboxylase (Tm1287) from *Thermotoga maritima* serendipitously solved in complex with oxalate (28) reveals bidentate binding of the oxalate, in contrast to the monodentate binding we observe in oxalate oxidase. Bidentate coordination is apparently non-productive in oxalate decarboxylase, since a productive substrate complex would not be stable in the enzyme. As discussed above, Leu^{77} and Met^{149} provide steric constraints on bidentate coordination in OXO. While it has not yet proven possible to prepare the oxalate complex in the crystal, the extended, monodentate coordination mode modeled by glycolate binding in the active site of OXO supports a mechanism for catalysis in which the manganese ion, together with Asn^{75}, Asn^{85}, and Gln^{139} comprise a redox active metal cofactor and hydrogen bonding framework that serves to activate substrates and orient intermediates during catalysis.

Acknowledgments—We acknowledge use of stations PX9.6 and PX14.1 at Synchrotron Radiation Source Daresbury and the Engineering and Physical Sciences Research Council's Chemical Database Service also at the Central Laboratory of the Research Councils Laboratory, Daresbury, UK.

REFERENCES

1. Sugiura, M., Yamamura, H., Hirano, K., Sasaki, M., Morikawa, M. & Tsuboi, M. (1979) *Chem. Pharm. Bull.* **27,** 2003–2007
2. Pietta, P. G., Calatroni, A., Agnellini, D. & Pace, M. (1982) *Prep. Biochem.* **12,** 341–353
3. Lane, B. G., Dunwell, J. M., Ray, J. A., Schmitt, M. R. & Cuming, A. C. (1993) *J. Biol. Chem.* **268,** 12239–12242
4. Koyama, H. (1988) *Agric. Biol. Chem.* **52,** 743–748
5. Aguilar, C., Urzũa, U., Koenig, C. & Vicuna, R. (1999) *Arch. Biochem. Biophys.* **366,** 275–282
6. Lane, B. G. (1994) *FASEB J.* **8,** 294–301
7. Zhou, F., Zhang, Z., Gregersen, P. L., Mikkelsen, J. D., Neurgaard, E., Collinge, D. B. & Thordahl-Christensen, H. (1998) *Plant Physiol.* **117,** 33–41
8. Dumas, B., Saill, A., Cheviet, J-P., Freyssinet, G. & Pallett, K. (1993) *C. R. Acad. Sci. (Paris)* **316,** 793–798
9. Dunwell, J. M., Purvis, A. & Khuri, S. (2004) *Phytochemistry* **65,** 7–17
10. Murzin, A. G., Brenner, S. E., Hubbard, T. & Chothia, C. (1995) *J. Mol. Biol.* **247,** 536–540
11. Woo, E. J., Dunwell, J. M., Goodenough, P. W. & Pickersgill, R. W. (1998) *FEBS Lett.* **437,** 87–90
12. Requena, L. & Bornemann, S. (1999) *Biochem. J.* **343,** 185–190
13. Woo, E. J., Dunwell, J. M., Goodenough, P. W., Marvier, A. C. & Pickersgill, R. W. (2000) *Nat. Struct. Biol.* **7,** 1036–1040
14. Whittaker, M. M. & Whittaker, J. W. (2002) *J. Biol. Inorg. Chem.* **7,** 136–145
15. Svedružić, D., Jónsson S., Toyota C. G., Reinhardt L. A., Ricagno S., Lindqvist Y. & Richards N. G. (2005) *Arch. Biochem. Biophys.* **433,** 176–192
16. Otwinowski, Z. & Minor, W. (1997) *Methods Enzymol.* **276,** 307–326
17. Leslie, A. G. W. (1992) *Joint CCP4 + ESF-EAMCB Newsletter on Protein Crystallography*, No. 26
18. Collaborative Computational Project Number 4 (1994) *Acta Crystallogr. Sect. D Biol. Crystallogr.* **50,** 760–767
19. Jones, T. A., Zou, J.-T., Cowan, S. W. & Kjeldgaard, M. (1991) *Acta Crystallogr. Sect. A,* **47,** 110–119
20. Fletcher, D. A., McMeeking, R. F. & Parkin, D. (1996) *J. Chem. Inf. Comput. Sci.* **36,** 746–749
21. Ellison, R. D., Johnson, C. K. & Levy, H. A. (1971) *Acta Crystallogr. Sect. B Struct. Sci.* **27**, 333–344
22. Vagin, A. & Teplyakov, A. (1997) *J. Appl. Crystallogr.* **30,** 1022–1025
23. Murshudov, G. N., Vagin, A. A. & Dodson, E. J. (1997) *Acta Crystallogr. Sect. D Biol. Crystallogr.* **53,** 240–255
24. Laskowski, R. A., MacAuthur, M. W., Moss, D. S. & Thornton, J. M. (1993) *Appl. Crystallogr.* **26,** 283–291
25. Whittaker, M. M., Ballou, D. P. & Whittaker, J. W. (1998) *Biochemistry* **37,** 8426–8436
26. Lobley, A., Whitmore, L. & Wallace, B. A. (2002) *Bioinformatics* **18,** 211–212
27. Lis, T. (1980) *Acta Crystallogr. Sect. B Struct. Sci.* **36**, 701–703
28. Schwarzenbacher, R., von Delft, F., Jaroszewski, L., Abdubek, P., Ambing, E., Biorac, T., Brinen, L. S., Canaves, J. M., Cambell, J., Chiu, H. J., Dai, X., Deacon, A. M., DiDonato, M., Elsliger, M. A., Eshagi, S., Floyd, R., Godzik, A., Grittini, C., Grzechnik, S. K., Hampton, E., Karlak, C., Klock, H. E., Koesema, E., Kovarik, J. S., Kreusch, A., Kuhn, P., Lesley, S. A., Levin, I., McMullan, D., McPhillips, T. M., Miller, M. D., Morse, A., Moy, K., Ouyang, J., Page, R., Quijano, K., Robb, A., Spraggon, G., Stevens, R. C., van den Bedem, H., Velasquez, J., Vincent, J., Wang, X., West, B., Wolf, G., Xu, Q., Hodgson, K. O., Wooley, J. & Wilson, I. A. (2004) *Proteins* **56,** 392–395
29. Kraulis, P. J. (1991) *J. Appl. Crystallogr.* **24,** 946–950
30. Esnouf, R. M. (1997) *J. Mol. Graph.* **15,** 132–134

Downloaded from www.jbc.org at KING'S COLLEGE LONDON on October 22, 2007